Optics Letters

Micro-cone arrays enhance outcoupling efficiency in horticulture luminescent solar concentrators

Zhijie Xu, Mark Portnoi, and Ioannis Papakonstantinou*

Photonic Innovations Lab, Department of Electronic and Electrical Engineering, University College London, London WC1E 7JE, UK
**Corresponding author: i.papakonstantinou@ucl.ac.uk*

Received 13 October 2022; revised 21 November 2022; accepted 21 November 2022; posted 23 November 2022; published 23 December 2022

Luminescent solar concentrators (LSCs) have shown the ability to realize spectral conversion, which could tailor the solar spectrum to better match photosynthesis requirements. However, conventional LSCs are designed to trap, rather than extract, spectrally converted light. Here, we propose an effective method for improving outcoupling efficiency based on protruded and extruded micro-cone arrays patterned on the bottom surface of LSCs. Using Monte Carlo ray tracing, we estimate a maximum external quantum efficiency (EQE) of 37.73% for our horticulture LSC (HLSC), corresponding to 53.78% improvement relative to conventional, planar LSCs. Additionally, structured HLSCs provide diffuse light, which is beneficial for plant growth. Our micro-patterned surfaces provide a solution to light trapping in LSCs and a foundation for the practical application of HLSCs.

https://doi.org/10.1364/OL.478206

With the continuous increase in population, the demand for food is surging, putting more pressure on global agriculture [1]. Crop yields are significantly affected by photosynthesis efficiency, which is associated with the photon spectrum [2]. In fact, only a narrow range of the solar spectrum benefits photosynthesis, mostly around the red wavelengths (600–700 nm) [3]. Conversely, some bands—such as ultraviolet and green light—even induce unexpected damage to crops, leading to production decrease or quality reduction [4].

Unfortunately, the peak intensity distribution of the AM1.5 spectrum does not match the preference for photosynthesis. The least efficient green component occupies the peak and accounts for 35% of the photosynthetically active range (PAR) of 400—700 nm [5]. One way to circumvent this disparity is by amplifying the red band at the expense of the green via luminescence. Luminescent solar concentrators (LSCs) consisting of polymer host matrices doped with fluorophores, can achieve this aim [6,7]. Fluorophores can absorb incident light and re-emit it by means of fluorescence [8,9]. By tuning the Stoke's shift, the re-emitted photon spectrum could be tailored to optimize photosynthesis [10–12].

Since the invention of LSCs in the 1970s [13,14], the field has experienced rapid growth [15–17]. However, most LSC devices are designed for photovoltaic applications [6,8] where it is beneficial to concentrate light by means of total internal reflection (TIR). Typically, light is emitted by the fluorophores isotropically; when the emission angle is greater than the critical angle, light falls within the TIR cone and is confined. For commonly used polymer hosts, a noticeable fraction (>70%) of photons end up being totally internally reflected [18]. In short, current LSCs are excellent photon concentrators, as their name suggests.

Consequently, even though LSC devices have shown potential for spectral conversion, if the outcoupling efficiency is poor, most of the converted photons would end up being trapped inside the polymer matrix and would never reach the plants. The Daily Light Integral (DLI), defined as the number of PAR photons per unit area received by plants within 24 hours, is a useful metric to evaluate crop yield [19]. Improving outcoupling efficiency would increase the DLI, thereby promoting production in a greenhouse. Recent advances on light extraction techniques for optical displays and LEDs provide possible avenues to boost outcoupling efficiency [20–23]. Intuitively, lowering the refractive index is the most obvious method to shrink the TIR cone and so push more light out of the device. In recent studies, this was achieved by inducing subwavelength porosity within the polymer matrix to create a medium with an effective index lower than its solid counterpart [24,25]. Alternatively, extrinsic structures, including microlenses [26], micro-pyramids [27], and micro-cones [28], were also reported to promote light extraction. Among them, micro-cone arrays achieve the best outcoupling efficiency on the condition of same area coverage and geometrical parameters [29].

In this Letter, we draw inspiration from light extraction features in LEDs and optical displays and apply them to the context of LSCs to improve outcoupling efficiency. We used Monte Carlo ray tracing, a technique widely used in LSC research [15,30–38], to analyze the performance of horticulture LSCs (HLSCs) (LightTools™, Optical Research Associates). In particular, we focus on hexagonally arranged micro-cone arrays on the bottom surface of LSCs due to their ability to frustrate TIR and deflect photons out of lightguides. Both extruding and protruding features are modeled and discussed. Effects of fluorophore concentration, HLSC thickness, and cone height/radius ratio (H/R) on photon fates are investigated.

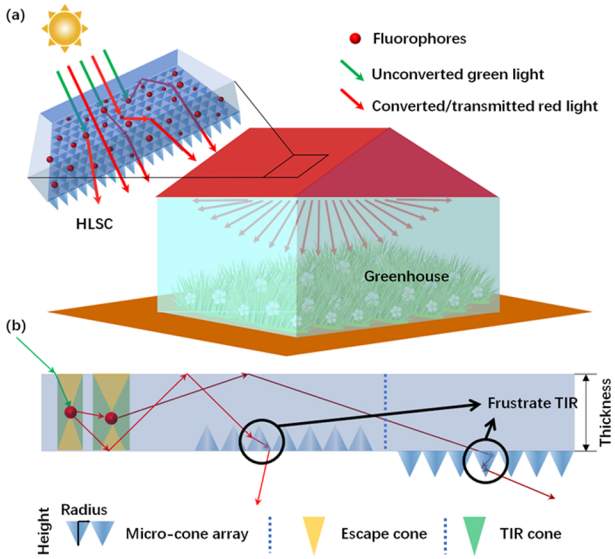

Fig. 1. (a) Schematic representation of a greenhouse HLSC with light extraction structures. (b) Concept of an HLSC improving light extraction. Green light is absorbed by fluorophores then converted into red light. Re-emitted light that fails to fall into the escape cone would be trapped in a planar LSC. Protruding and extruding micro-cone arrays frustrate TIR, however, and improve outcoupling efficiency.

Before discussing the modeling results, some metrics should be established for evaluating outcoupling efficiency. Note that the metrics used here are not the same as the ones in conventional LSCs, reflecting the different nature of our problem. Firstly, internal quantum efficiency (IQE) is defined as the ratio of photons escaping from the *bottom* surface to the total number of photons absorbed (see Fig. 1). This parameter characterizes the ability to extract the converted photons from the bottom surface, which is the useful surface emitting toward the plants (photons leaving from the top and side surfaces are considered lost). The second parameter is the external quantum efficiency (EQE) defined as the ratio of photons escaping from the bottom surface to the *total* number of incident photons. EQE marks the total utilization rate of solar energy.

Figure 1(a) illustrates the schematic diagram of the HLSC whereby green light is first redshifted before being emitted toward the interior of the greenhouse to facilitate photosynthesis. In our simulations, we used an artificial polymer matrix with a refractive index of 1.5 (common for polymers used in LSC research [18]) and a prototypical fluorescent dye, Lumogen Red—an economical dye with high quantum yield (96%)—widely adopted in LSC research. The absorption spectrum of Lumogen Red peaks at 575 nm and the re-emitted light spans the wavelength range from 570 to 700 nm [39] making it ideal for photosynthesis enhancement.

Figure 1(b) illustrates the mechanism of light extraction. Re-emitted photons reach the bottom, polymer–air interface. If the incident angle is smaller than the critical angle θ_c defined by Snell's law:

$$\theta_c = \sin^{-1}\left(\frac{n_{air}}{n_{LSC}}\right),$$

where n_{air} and n_{LSC} are refractive indexes of air and the host matrix, respectively, the photons fall into the escape cone [depicted by orange triangles in Fig. 1(b)] and leave the device. Otherwise, photons are trapped due to TIR [green triangles in Fig. 1(b)]. Considering the refractive index is 1.5 in our simulations, the corresponding critical angle is ~42°. Accounting for the solid angle subtended by the TIR cone, the portion of trapped photons is given by

$$\eta = \frac{\int_0^{2\pi}\int_{\theta_c}^{\pi-\theta_c}\sin(\theta)d\theta d\phi}{4\pi} = \cos(\theta_c).$$

As a result, the trapping efficiency is ~74%. To reduce light trapping, micro-extraction features patterned on the bottom surface are proposed to frustrate the TIR process in the HLSC device. As shown in Fig. 1(b), both protruding and extruding micro-cone arrays are considered, as both can easily be made by scalable fabrication methods such as nanoimprint lithography, roll-to-roll hot-embossing, or others [40]. The key geometrical and material parameters to examine are the H/R, the thickness of the device, and the fluorophore concentration in the host polymer. The performance of sparser, non-touching base cone arrays is consistently worse than with touching bases due to the lower coverage area. So, to achieve the highest density, the micro-cones are arranged in a hexagonal manner with touching bases.

Based on the definitions of EQE and IQE, the following relationship can be derived connecting these two key metrics:

$$\frac{EQE}{IQE} = \left(1 - \frac{Fresnel\ Loss}{Input\ photons}\right) \times Absorbance.$$

Fresnel Loss accounts for ~4%, when the refractive index is 1.5 and incident angle is normal [41], so the first term on the right-hand side of the equation is ~1. Thus EQE is approximately equal to the product of the absorbance and IQE.

To optimize the EQE, we chose to work with a monochromatic light source at 520 nm. While this wavelength falls in the absorption spectrum, it avoids the emission spectrum, which is convenient for photon fate calculation as we have shown in our previous work [15]. The area of the HLSC was fixed to 80×80 mm (thickness varying from 1 to 6 mm), both because this is compatible with small-scale experimental prototypes [34], but also because results remain essentially the same for larger dimensions. The fluorophore concentration used in our simulations ranged from 2×10^{-6} M to 1×10^{-4} M, equivalent to absorbance ranging from 0.026 to 0.855 through the LSC thickness. Furthermore, our simulations verified that EQE remains invariant to radius changes from 10 μm to 1 mm when the H/R ratio remains constant. As such we decided to fix the radius to 50 μm, a value easily attainable.

As shown in Fig. 2(a), IQE shows a monotonic increase with H/R in the examined range from 0 to 4. Note that H/R = 0 implies a planar device and is used here for comparison with the micro-cones. H/R = 4 corresponds to a very sharp cone and was taken as the limit since larger values did not show further improvement. A plateau actually starts appearing already at H/R~0.8, indicating that light extraction efficiency is saturated. This is the critical value beyond which most TIR rays meet the micro-cone facets at a sufficiently acute angle to cause their extraction [see Fig. 1(b)]. As all converted photons are assumed to be emitted isotropically, IQE depends more on the geometrical parameters of the micro-cones and less on the device thickness and fluorophore concentration. The highest IQEs for samples of thickness 1, 2, 3, 4, 5, and 6 mm are 49%, 45%, 43%, 41%, 39%, and 38%, respectively. An IQE with a maximum increase of about 119%, compared with a planar LSC, is achieved for

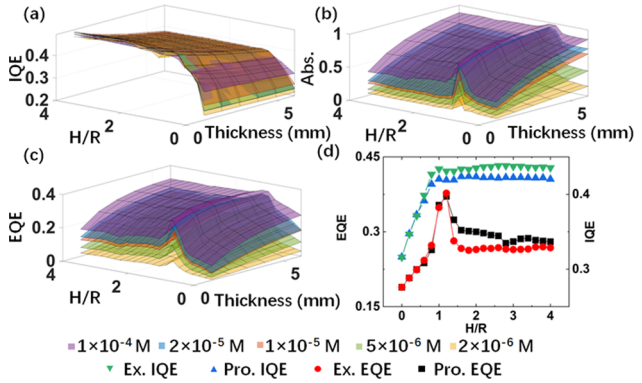

Fig. 2. Simulated (a) IQE, (b) absorbance (Abs.), and (c) EQE as a function of H/R, HLSC thickness, and fluorophore concentration for extruding structures. (d) Comparison of IQE and EQE for extruding and protruding structures.

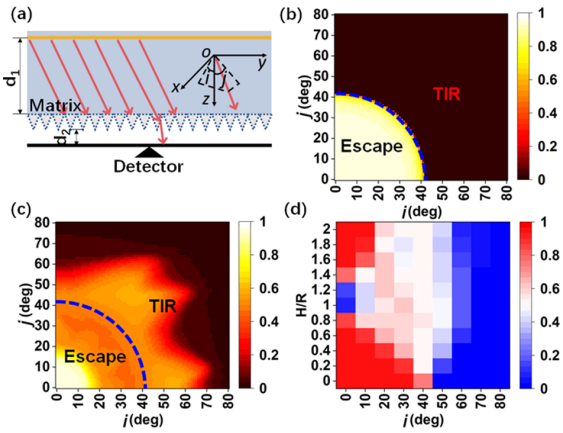

Fig. 3. (a) Simulation model used for testing micro-cone arrays enhancing light extraction. Outcoupling efficiency as a function of incident angle detected from (b) planar polymer slab, and (c) micro-cone array slab for H/R = 1.2. The blue dashed line delineates the end of the escape cone and the beginning of the TIR cone. Only one quadrant is simulated due to the symmetry of cones. (d) Detected outcoupling efficiency for different incident angles i and H/R.

H/R = 3 when the concentration is 2×10^{-6} M and thickness is 1 mm. Variation of absorbance shows a distinctly different trend. As shown in Fig. 2(b), thickness, fluorophore concentration, and H/R all noticeably affect absorbance. Increasing fluorophore concentration, for example, reduces the mean free path for absorption. As a result, the probability that a photon is absorbed increases. Thicker samples, on the other hand, lengthen the optical path light travels in the device, again amplifying photon absorbance. In addition, the cone structure may also back-reflect some unabsorbed photons, providing them with yet another chance to be absorbed. Take the example of near normal incidence. When H/R = 1 (cone tip angle of 90°), most unabsorbed photons reaching the bottom textured surface will be back-reflected, doubling the optical path in the device. In this case, significant improvements compared to the planar LSC can be attained, as exemplified in Fig. 2(b).

As well as benefiting from an increase in IQE and absorbance, the micro-cone arrays significantly improve the EQE. According to Fig. 2(c), EQE closely tracks the variation of absorbance, particularly for the higher H/R for which IQE saturates. The highest EQE achieved is 37.73% for H/R = 1.2, concentration 1×10^{-4} M, and sample thickness 3 mm. This corresponds to a 53.78% improvement compared with the best results obtained with a planar LSC. According to the simulation results from Fig. 2(d), the protruding structures show a similar performance with the extruding, offering flexibility in future HLSC device fabrication.

To shed more light on how micro-cones frustrate TIR, we ran the additional simulations summarized in Fig. 3. In this case, we positioned a plane wave source inside a micro-cone textured polymer slab which was clear, i.e., not doped with fluorophores. Then we monitored the portion of photons escaping the bottom surface as a function of the incident angle by placing a detector just underneath the micro-cones [Fig. 3(a)]. Note that H/R is set as 1.2 here, the value at the highest EQE is achieved. At the top of the polymer slab, a perfectly absorbing layer was placed to stop all rays not extracted by the micro-cones and remove them from the simulation region. For comparison, we repeated the same simulations for a planar slab. Outcoupling efficiency (i.e., the ratio of photons escaping from a certain incident angle over the initial number of photons emitted at this angle) is plotted in Figs. 3(b) and 3(c) as a function of incident angles (i, j), where i and j represent the orientations in X–Z and Y–Z plane, respectively, as shown in Fig. 3(a). According to Fig. 3(b), only incident angles that are smaller than the critical angle escape in the planar slab case (escape zone), as expected. The behavior of micro-cones is strikingly different, though. According to Fig. 3(c), the angular distribution of rays exiting the textured surface extends far into the TIR zone (TIR limits are represented by the blue dashed line). As a matter of fact, the outcoupling efficiency is sustained to >0.4 for incident angles even greater than 60°, and it never drops to zero even for nearly grazing angles. This expansion of extracted angles beyond the escape cone is the principal mechanism of outcoupling efficiency improvement in our system. Variation of outcoupling efficiency based on H/R and incident angle i (j is fixed as 0°) is concluded in Fig. 3(d). For all H/R, extraction angles always extend beyond TIR, verifying that micro-cones are an effective way of improving outcoupling efficiency.

Once micro-cones were optimized for optimum outcoupling efficiency, new simulations were run to account for the entire AM1.5 spectrum. Figure 4(a) shows the spectral distribution of light escaping from the bottom of the device for (i) a planar LSC and (ii) a micro-cone HLSC. All results were normalized to the peak value of the micro-cone HLSC spectrum. In these simulations, the thickness of the device was 5 mm and fluorophore concentration was 1×10^{-4} M, corresponding to the values showing best performance. Both planar LSC and micro-cone HLSC show a significant reduction of the power in the green band and concomitant energy transfer to the red. Compared with its planar counterpart, a micro-cone HLSC shows an increased power of 11.8% in the red. However, this improvement is somewhat lower than that of EQE (~53.78%, as discussed before). This is attributed to the back-reflection from the unabsorbed red component in the AM1.5 spectrum. Despite this, power in the red area from a structured HLSC is still 52.58% higher than that from the AM1.5 spectrum.

Finally, it is noted that diffuse light is preferable as it can reach not only the leaves but also the stems and roots of plants [42] [Fig. 4(b)], and as found, the micro-cone HLSC acts as excellent light diffuser too. Figure 4(c) shows the angular distribution of light escaping from a planar LSC. Figure 4(d), on the other hand, illustrates the angular profile of photons escaping the micro-cone

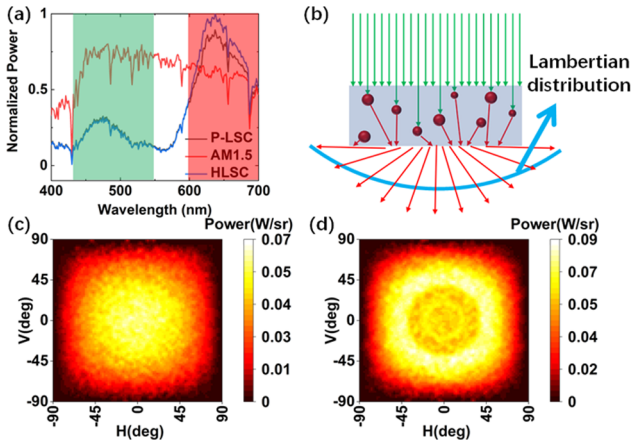

Fig. 4. (a) Normalized radiant power escaping planar LSC and micro-cone HLSC and comparison with the AM1.5 spectrum. Green area represents spectral band of poor photosynthesis efficiency, while red area represents band of high efficiency. (b) Concept of HLSC providing diffuse light for plant growth. Simulated angular distribution of radiant intensity for (c) planar LSC, and (d) micro-cone HLSC. Angles V and H are based on the Type B coordinate system for a Goniophotometer.

HLSC. For both cases, the angular profile resembles a Lambertian distribution, showing that the extra outcoupling efficiency in micro-cone HLSCs is not impacting photon randomization.

In summary, LSCs with patterned micro-cone arrays were optimized for light extraction using the Monte Carlo ray-tracing method. The morphology of the micro-cone arrays was investigated by controlling the H/R to obtain the best IQE and absorbance, thereby facilitating the improvement of EQE. Combined with sample thickness and fluorophore concentration optimization, the highest EQE of 37.73% could be achieved, corresponding to 11.8% more red light reaching the plants compared to an equivalent planar LSC. Simultaneous spectral conversion, enhanced light extraction, and light diffusion were realized with our micro-cone HLSC device, showing great potential for horticulture applications. In the future, efforts will be focused on designs that do not affect the original red spectrum, for example by texturing both surfaces of the LSC. The top surface could be textured with nano-cone arrays [43,44] that act as anti-reflection layers or with other micro-cone geometries.

Funding. China Scholarship Council (202009110161); UCL Engineering, University College London (Dean's prize) .

Disclosures. The authors declare no conflicts of interest.

Data availability. Data underlying the results presented in this paper are not publicly available at this time but may be obtained from the authors upon reasonable request.

Supplemental document. See Supplement 1 for supporting content.

REFERENCES

1. D. K. Ray, N. D. Mueller, P. C. West, and J. A. Foley, PLoS One **8**, e66428 (2013).
2. M. D. Ooms, C. T. Dinh, E. H. Sargent, and D. Sinton, Nat. Commun. **7**, 12699 (2016).
3. L. Wondraczek, M. Batentschuk, M. A. Schmidt, R. Borchardt, S. Scheiner, B. Seemann, P. Schweizer, and C. J. Brabec, Nat. Commun. **4**, 2047 (2013).
4. K. Ravindran, A. Indrajith, P. Pratheesh, K. Sanjiviraja, and V. Balakrishnan, Int. J. Eng. Sci. Tech. **2**, 226 (2010).
5. L. Shen, R. Lou, Y. Park, Y. Guo, E. J. Stallknecht, Y. Xiao, D. Rieder, R. Yang, E. S. Runkle, and X. Yin, Nat. Food **2**, 434 (2021).
6. R. A. S. Ferreira, S. F. H. Correia, A. Monguzzi, X. Liu, and F. Meinardi, Mater. Today **33**, 105 (2020).
7. B. McKenna and R. C. Evans, Adv. Mater. **29**, 1606491 (2017).
8. M. G. Debije and P. P. C. Verbunt, Adv. Energy Mater. **2**, 12 (2012).
9. A. Kim, A. Hosseinmardi, P. K. Annamalai, P. Kumar, and R. Patel, ChemistrySelect **6**, 4948 (2021).
10. M. Hammam, M. K. El-Mansy, S. M. El-Bashir, and M. G. El-Shaarawy, Desalination **209**, 244 (2007).
11. F. Meinardi, A. Colombo, K. A. Velizhanin, R. Simonutti, M. Lorenzon, L. Beverina, R. Viswanatha, V. I. Klimov, and S. Brovelli, Nat. Photonics **8**, 392 (2014).
12. J. Keil, Y. Liu, U. Kortshagen, and V. E. Ferry, ACS Appl. Energy Mater. **4**, 14102 (2021).
13. A. Goetzberger and W. Greube, Appl. Phys. **14**, 123 (1977).
14. W. H. Weber and J. Lambe, Appl. Opt. **15**, 2299 (1976).
15. C. Tummeltshammer, A. Taylor, A. J. Kenyon, and I. Papakonstantinou, Sol. Energy Mater. Sol. Cells **144**, 40 (2016).
16. I. Papakonstantinou, M. Portnoi, and M. G. Debijie, Adv. Energy Mater. **11**, 2002883 (2021).
17. M. G. Debije, R. C. Evans, and G. Griffini, Energy Environ. Sci. **14**, 293 (2021).
18. F. Jabeen, M. Chen, B. Rasulev, M. Ossowski, and P. Boudjouk, Comput. Mater. Sci. **137**, 215 (2017).
19. J. E. Faust, V. Holcombe, N. C. Rajapakse, and D. R. Layne, HortSci. **40**, 645 (2005).
20. S. Amoah, X. Fu, S. Yin, Q. Dong, C. Dong, and F. So, ACS Appl. Mater. Interfaces **14**, 9377 (2022).
21. P. Mao, C. Liu, X. Li, M. Liu, Q. Chen, M. Han, S. A. Maier, E. H. Sargent, and S. Zhang, Light: Sci. Appl. **10**, 180 (2021).
22. Y. Sun and S. R. Forrest, Nat. Photonics **2**, 483 (2008).
23. Y. Qu, M. Slootsky, and S. R. Forrest, Nat. Photonics **9**, 758 (2015).
24. J. K. Kim, S. Chhajed, M. F. Schubert, E. F. Schubert, A. J. Fischer, M. H. Crawford, J. Cho, H. Kim, and C. Sone, Adv. Mater. **20**, 801 (2008).
25. M. Slootsky and S. R. Forrest, Opt. Lett. **35**, 1052 (2010).
26. S. Möller and S. R. Forrest, J. Appl. Phys. **91**, 3324 (2002).
27. H. Greiner, Jpn. J. Appl. Phys. **46**, 4125 (2007).
28. J. H. Son, J. U. Kim, Y. H. Song, B. J. Kim, C. J. Ryu, and J. L. Lee, Adv. Mater. **24**, 2259 (2012).
29. P. Kumar, S. Y. Son, R. Singh, K. Balasundaram, J. Lee, and R. Singh, Opt. Commun. **284**, 4874 (2011).
30. C. Tummeltshammer, M. S. Brown, A. Taylor, A. J. Kenyon, and I. Papakonstantinou, Opt. Express **21**, A735 (2013).
31. C. Tummeltshammer, A. Taylor, A. J. Kenyon, and I. Papakonstantinou, J. Appl. Phys. **116**, 173103 (2014).
32. I. Papakonstantinou and C. Tummeltshammer, Optica **2**, 841 (2015).
33. M. Rafiee, S. Chandra, H. Ahmed, K. Barnham, and S. J. McCormack, Opt. Express **29**, 15031 (2021).
34. M. Portnoi, T. J. Macdonald, C. Sol, T. S. Robbins, T. Li, J. Schläfer, S. Guldin, I. P. Parkin, and I. Papakonstantinou, Nano Energy **70**, 104507 (2020).
35. M. Portnoi, P. A. Haigh, T. J. Macdonald, F. Ambroz, I. P. Parkin, I. Darwazeh, and I. Papakonstantinou, Light: Sci. Appl. **10**, 3 (2021).
36. C. Tummeltshammer, A. Taylor, A. J. Kenyon, and I. Papakonstantinou, Opt. Lett. **41**, 713 (2016).
37. M. Portnoi, C. Sol, C. Tummeltshammer, and I. Papakonstantinou, Opt. Lett. **42**, 2695 (2017).
38. C. Tummeltshammer, M. Portnoi, S. A. Mitchell, A. T. Lee, A. J. Kenyon, A. B. Tabor, and I. Papakonstantinou, Nano Energy **32**, 263 (2017).
39. L. Desmet, A. J. M. Ras, D. K. G. de Boer, and M. G. Debije, Opt. Lett. **37**, 3087 (2012).
40. T. Velten, F. Bauerfeld, H. Schuck, S. Scherbaum, C. Landesberger, and K. Bock, Microsyst. Technol. **17**, 619 (2011).
41. J. D. Jackson and R. F. Fox, Am. J. Phys. **67**, 841 (1999).
42. T. Li and Q. Yang, Front. Plant Sci. **6**, 1 (2015).
43. M. Michalska, S. K. Laney, T. Li, M. K. Tiwari, I. P. Parkin, and I. Papakonstantinou, Nanoscale **14**, 1847 (2022).
44. M. Michalska, S. K. Laney, T. Li, M. Portnoi, N. Mordan, E. Allan, M. K. Tiwari, I. P. Parkin, and I. Papakonstantinou, Adv. Mater. **33**, 2102175 (2021).